

## Investigation of Thermal Performance of Electric Vehicle BLDC Motor

James Kuria<sup>1,1</sup>, Pyung Hwang<sup>2</sup>,

<sup>1</sup>Department of Mechanical Engineering, Jomo Kenyatta University of Agriculture & Technology, P.O. Box 62000-00200, Nairobi, Kenya

<sup>2</sup>School of Mechanical Engineering, Yeungnam University, Gyeongsan 712-749, Republic of Korea

[jkuria@eng.jkuat.ac.ke](mailto:jkuria@eng.jkuat.ac.ke), [phwang@yu.ac.kr](mailto:phwang@yu.ac.kr)

**Abstract.** Overreliance on petroleum products and environmental pollution from combustion emissions produced by automobiles has led to extensive research on hybrid electric vehicles, electric vehicles and their components. A key component in these vehicles is the electric motor, used for traction as well as powering other appliances like the compressor. Overheating in electrical motors results in detrimental effects such as degradation of the insulation materials, magnet demagnetization, increase in Joule losses and decreased motor efficiency and lifetime. Hence, it is important to find ways of optimizing performance and reliability of electric motors through effective cooling and consequently reduce operating and maintenance costs. This study describes 3D CFD simulations performed on a totally enclosed air over fan cooled brushless D.C. motor to identify the temperatures of the critical components of the motor, and the effect of varying thermal parameters of these temperatures. The energy sources are obtained from electromagnetic losses computed using MAXWELL, a commercial FEA software and bearing losses obtained through numerical methods developed by the authors. A finned casing is used as the heat sink and the effect of varying the fin geometry on the cooling performance is examined using three heat sink designs. The results show that the highest temperature occurs at the end windings and that this temperature can be reduced by up to 15% by introduction of a suitable finned housing. These results show that CFD can be effectively used to optimize the cooling performance of electric motors. Experimental tests are undergoing in order to validate the CFD results..

**Keywords:** BLCD motor, bearing frictional losses, CFD analysis, electromagnetic losses, thermal performance

---

<sup>1</sup> Corresponding Author

## 1 Introduction

Brushless DC (BLDC) permanent magnet (PM) motors are increasingly being employed in electric vehicles (EV) and hybrid electric vehicles (HEV), due to their high efficiency, high power density and minimal maintenance [1]. The ability of BLDC motor to function as generators during regenerative braking makes it ideal for EV applications.

Motor temperature is closely linked to the life and performance of BLDC motor. Stator winding temperature directly affects the winding insulation system's durability while the rotor temperature affects the efficiency of the permanent magnets [2]. Overheating in the windings increases joule's losses, since the electrical resistance of the winding material is highly temperature dependent [2]. It is therefore imperative to conduct thermal analysis in the design of BLDC motors. Heat generated within an electric motor comes from two primary sources: electromagnetic losses and mechanical losses. Electromagnetic losses consist of joules losses due to flow of electric current and core losses due to hysteresis effect. Mechanical losses consist of bearing frictional losses and windage losses [3].

Most recent advances in thermal modeling of electrical machines include lumped parameter thermal circuits, finite element method (FEM) and computational fluid dynamics (CFD) [4-6]. With use of a proper thermal network, the temperature of different parts of an electrical machine can be predicted with an acceptable accuracy [6]. Boglietti, et al., [7], investigated the thermal behavior of TEFC induction motors using commercial software, MotorCAD, and verified the models experimentally. The results showed an accuracy of  $\pm 5^\circ$  C on the winding temperature, which would be acceptable for most applications. Wallerand and Laurent [4], studied the thermal behavior of a permanent magnet (PM) motor at steady state and during a short-circuit using thermal networks. They also analyzed the performance of the motor using FEM simulations in Flux 2D, a commercial FEM software. The results showed that under thermal steady state under maximum torque, the temperature of the rotor is not high enough to present demagnetization problems. Other studies that have employed thermal networks in analysis of electrical machines include [8-10]. Thermal network models are preferred for their simplicity, compactness and are computationally inexpensive. However, they are characterized by low accuracy, and do not lend themselves to optimizing thermal parameters such as heat sink geometry, thermal contact resistance and fan geometry.

CFD has also received appreciable attention from various authors in thermal analysis of electric motors. Chih-Chung, et al. [11], carried out experimental and numerical investigations on motor cooling performance. Their aim was to determine pressure rise-flow rate (P-Q) performance curves of axial flow and centrifugal fans operating at 1800 rpm and to calculate the temperature distribution of the stator and rotor. They

also presented a discussion on how to improve motor cooling performance. Other authors, [2, 12, 13], have employed CFD to study thermal performance of electrical motors and the effect of various thermal parameters on cooling performance. In most of these studies, the heat source has been assumed to be evenly distributed within the generating components, which is usually not the case, as shown in Fig. 1 [3]. In addition, the effect of heat sink geometry on the cooling performance has not been adequately explored using CFD. The heat generated due to bearing friction loss is normally neglected in most cases. Hwang and Kuria [3], showed that bearing losses account for close to 10% of the total motor losses. These losses are dissipated in form of heat and should be included in thermal analysis of electric motors.

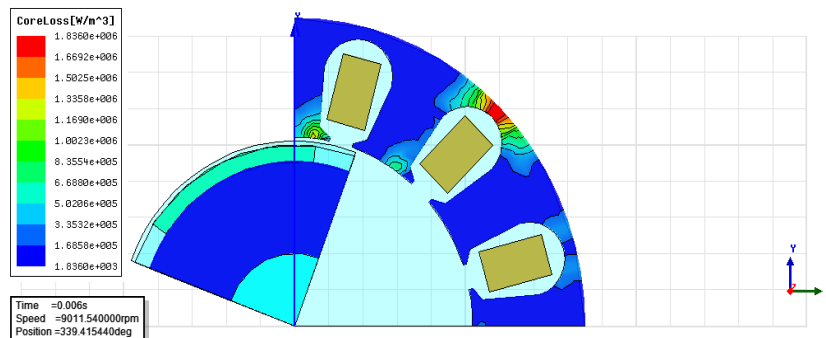


**Fig. 1.** Contours of coreloss in a BLDC motor, obtained from MAXWELL simulations.

This study therefore aims at investigating the thermal performance of a 1.2 kW brushless DC permanent magnet motor and examining the effect of heat sink (motor housing) geometry on the cooling performance of the motor. The motor is composed of an axial fan, a shaft, a stator, a rotor with permanent magnets, stator windings, motor housing, a front cover and two rolling element bearings. The specifications of the motor are shown in Table 1. The motor is to be used to power the electric vehicle compressor. Commercial CFD software, ANSYS FLUENT was employed in the analysis.

**Table 1.** Motor properties.

Parameter	Value
Type	BLDC PM motor
Power rating	1.2 kW
Maximum speed	13,000 rpm
Rated speed	8,000 rpm
Rated torque	1.5 Nm
Voltage	DC 72 V

Housing diameter	120 mm
------------------	--------

## 2 Modeling Motor Losses

Power losses in BLDC motors are an important consideration as they are dissipated in form of heat and hence they act as energy sources in computational fluid dynamics (CFD) analysis. Motor losses consist of electromagnetic and mechanical losses

### 2.1 Electromagnetic Losses

Electromagnetic losses consist of four main components:

1. Winding copper losses  $P_{cu}$  that are caused by resistive heating of the copper windings and are defined by:

$$P_{cu} = 3R_{\theta}I_{rms}^2 \quad (1)$$

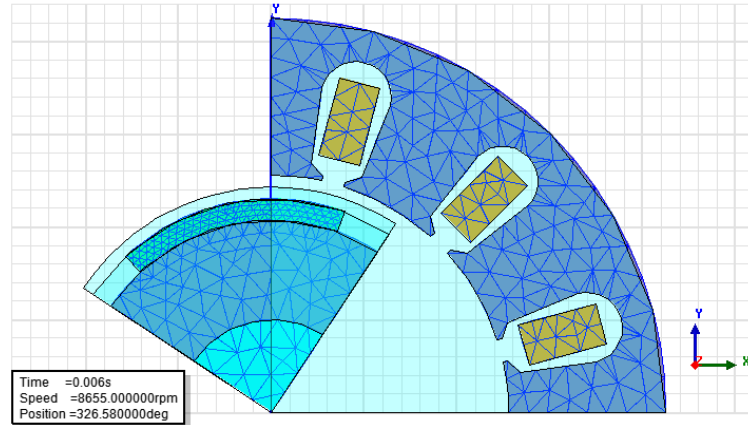
where  $R_{\theta}$  and  $I_{rms}$  are respectively the winding phase resistance and the RMS value of the motor phase current.

2. Core losses  $P_{fe}$ , consist of eddy current losses and hysteresis effect. In brushless DC motors, the variation of flux in the stator core is not sinusoidal and hence the iron core loss is given by:

$$P_{fe} = k_h f \hat{B}^{\alpha} + \frac{k_e}{2\pi^2} \left\{ \frac{dB}{dt} \right\}_{rms}^2 \quad (\text{W/kg}) \quad (2)$$

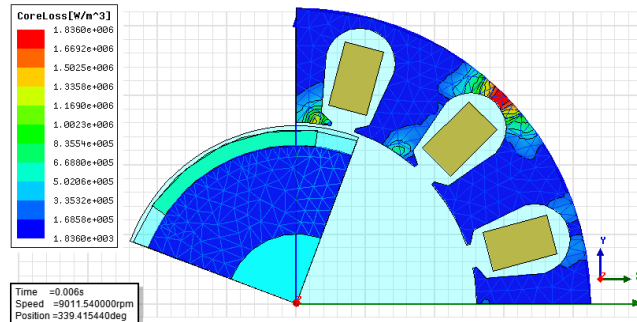
Where the first term is the hysteresis loss and the second is the eddy current loss.  $\hat{B}$  is the peak value of the flux density and  $f$ ,  $k_h$ ,  $\alpha$  and  $k_e$  are constants determined by curve fitting from manufacturer's data [14].

The electromagnetic losses were obtained using Ansoft Maxwell that employs finite element analysis. Due to periodicity of the motor, only  $\frac{1}{4}$  of the motor was analyzed in order to reduce the computational requirements. Figure 2 shows the 2D FEA mesh of  $\frac{1}{4}$  of the motor used in the study.



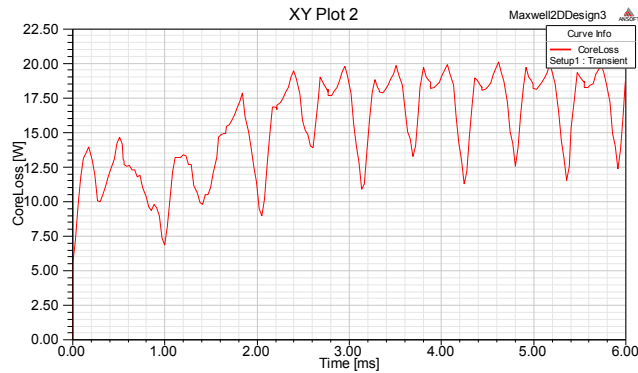
**Fig. 2.** 2D FEA mesh in Ansoft MAXWELL.

Fig. 3 shows contour plots of the core loss obtained from MAXWELL simulations.



**Fig. 3.** Contours of coreloss in a BLDC motor, obtained from MAXWELL simulations.

Fig. 4 and 5 show transient core and stranded copper losses respectively. The core loss is dependent on rotor and stator material properties while stranded loss is directly proportional to the current density. Stranded windings were employed in the analysis in order to simplify the computations.



**Fig. 4.** Transient stator core loss.

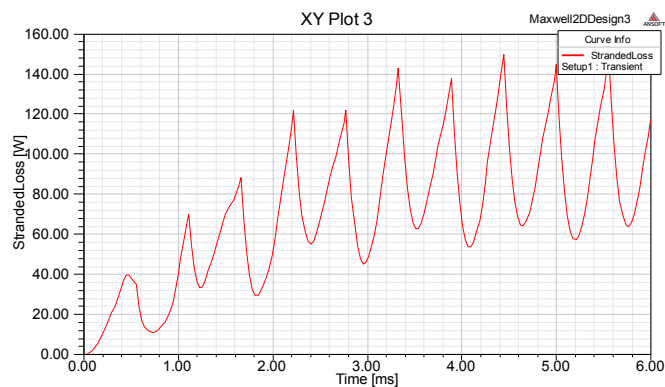


**Fig. 5.** Transient stranded copper loss.

## 2.2 Bearing Losses

Bearing friction losses consist of four main components [15]:

1. Hydrodynamic rolling force.
2. Sliding friction losses between the rolling elements and the races.
3. Sliding friction between the rolling elements and the separator/ cage.
4. Hysteresis losses – energy lost due to repeated cycles of deformation and recovery.

The bearing losses were computed using methods presented by Hwang and Kuria [3]. Fig. 6 shows the variation of the total bearing loss as a function of angular displacement. The fluctuations of the loss are due to the change in the number of rolling elements within the load carrying zone.

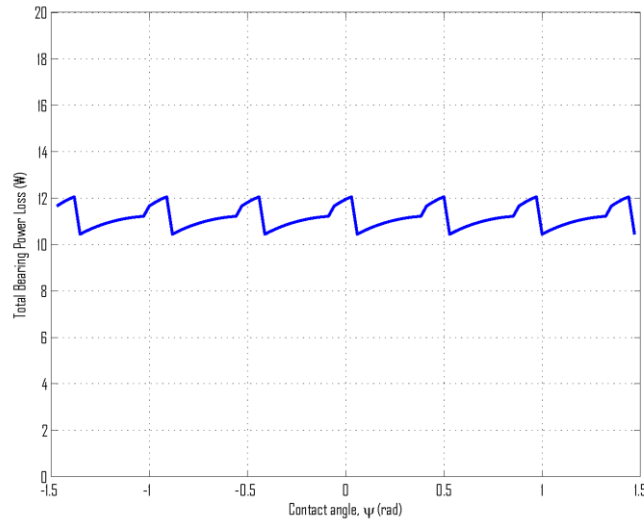


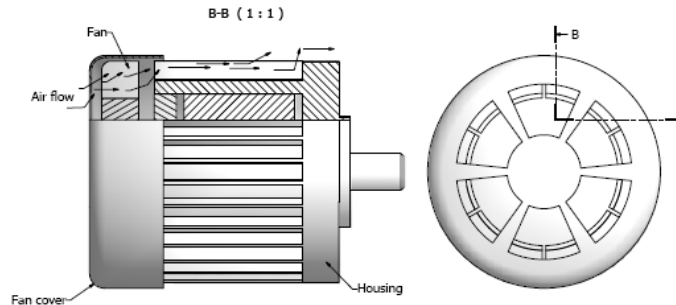
**Fig. 6.** Bearing friction loss across the loading zone.

### 3 CFD Model Formulation

#### 3.1 Computational Domain

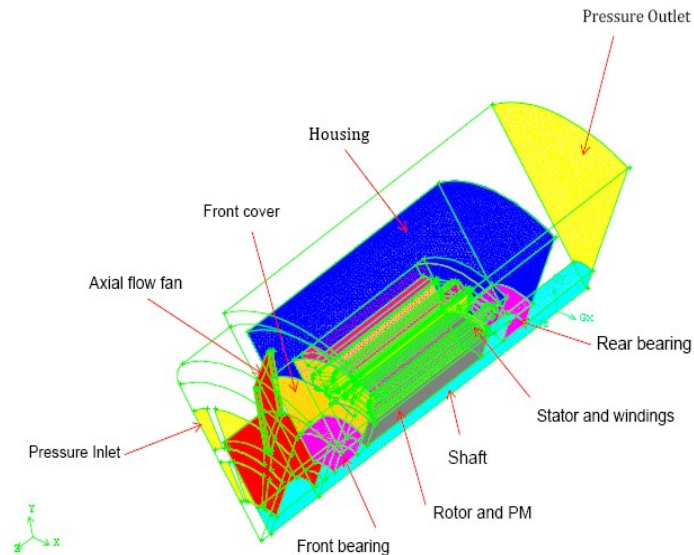
The motor geometry was created using GAMBIT, FLUENT's pre-processor. Model detail includes; the external housing geometry, front cover, stator core geometry including slot detail, stator windings, rotor geometry including permanent magnets, shaft, fan and fan cover. The fan cover includes the inlet slots for the air inlet. The fan cover creates a pressure drop that prevents the flow from spilling back out of the inlet. A tube axial fan is used to blow the air over the motor housing. The winding is modeled as a solid section in order to simplify the model and reduce the set-up and computational time.

Fig. 7 shows a front and side view of the motor geometry. Air enters through the opening slots on the fan cover, passes through the fan and to the housing. The rotor, stator, windings and the insulation are totally enclosed to protect them from moisture and dust which may affect durability and the overall performance of the motor [16].



**Fig. 7.** Orthographic views of the BLDC motor.

Taking advantage of the periodicity of both the flow and the geometry, it is sufficient to model one-sixth of the motor. This reduces the computational time and memory. Fig. 8 shows the model geometry and mesh of one-sixth of the whole motor. A fluid zone is created for the air enclosing the fan, within the motor (air gap and end spaces) and surrounding the housing. An additional fluid domain has been added outside the housing fluid due to the absence of an enclosure.



**Fig. 8.** Geometry and mesh of one-sixth of the BLDC motor.

### 3.2 Boundary Conditions

At the fan inlet, air is sucked from the atmosphere and hence a pressure inlet boundary with zero gauge pressure is applied at the fan upstream. Moving reference frame rotating at the fan speed is assigned to the fluid enclosing the fan while the fan and hub walls are assigned moving walls with zero slip and zero relative velocity with respect to the surrounding zones. The fan creates a static pressure rise within the fluid which then flows past the housing and exits at the pressure outlet with zero static pressure since the air is dissipated to the atmosphere. The rotor wall, shaft wall and magnet walls are assigned moving walls with zero relative velocity with respect to the surrounding zone. The symmetry cross-sections are assigned periodic boundaries. A hybrid mesh containing 1015712 tetrahedral and hexahedral cells was created for the simulation.

The electromagnet losses obtained from MAXWELL simulations and bearing losses obtained from numerical models [3] were used as energy sources. Table 2 shows the various motor losses computed for the BLDC motor in this study. The stator was divided into three zones; the stator body, teeth and tip and the stator coreloss assigned to these zones. The rotor coreloss and bearing losses were assumed to be evenly distributed in these components. The stator lining and winding insulation were assigned thin wall with an effective thermal conductivity.

**Table 2.** Motor losses and corresponding heat sources

Loss	Value	Heat source (W/m <sup>3</sup> )
Coreloss	50 W	Stator teeth
		Stator tip
		Stator body
		Rotor
Copper losses	150 W	3,000,000
Bearing friction loss	12 W	450,000

### 3.3 Solution Method

The commercial CFD package fluent was used to solve the Reynolds Averaged Navier Stokes Equations. Due to the high Reynolds number within the fan zone ( $Re = 110,000$ ), based on the chord length of the fan blade as shown in equation 1, standard  $k - \varepsilon$  turbulence model was employed to handle the turbulent flow within this region.

$$Re = \frac{\rho v L}{\mu} \quad (3)$$

Where L is the chord length of the blade and v is the relative velocity of the fluid.

The steady state energy equation was solved in the entire domain consisting of the fluid plus the solid in the form:

$$\nabla \cdot (\vec{V} \rho h) = \nabla \cdot (k \nabla T) + S_h \quad (4)$$

Where  $k$  is the thermal conductivity  $S_h$  is the volumetric heat source and  $h$  is the sensible enthalpy given by:

$$h = \int_{T_{ref}}^T c_p dT \quad (5)$$

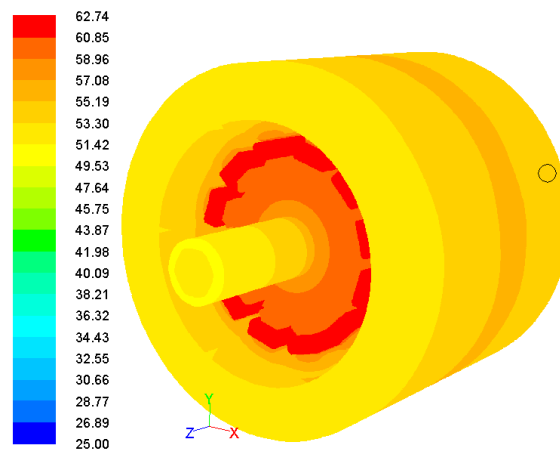
The momentum and continuity equations were solved in the fluid domain. The appropriate material properties were considered for each solid and fluid in the system.

Residues less than  $10^4$  were used as the convergence criteria for continuity, velocity, energy and turbulence quantities ( $k$  and  $\varepsilon$ ). The models demanded an average of 900-1200 iterations to converge.

#### 4 Results and Discussions

The main aim of this study was to evaluate the effectiveness of fin geometry in optimizing thermal parameters of electric motors. In this study, four geometries of the housing were used as the heat sink and their effectiveness in heat dissipation compared. The design goal was to have the simplest geometry possible so as to reduce the manufacturing cost and hence, the first geometry considered was a cylindrical housing. The introduction of fins should justify the cost and complexity associated with fins [17].

Fig. 9 shows contours of temperature on the shaft, rotor, stator, winding and motor housing. The temperature contours illustrate heat influx to these components from the bearings, rotor, winding and stator.



Contours of Static Temperature (c)

**Fig. 9.** Contours of temperature on the shaft, rotor, stator, windings and housing.

The highest temperature is observed at the windings and insulation area which could be attributed to the low thermal conductivity of the insulation and stator teeth lining. The temperature on the housing and stator increases towards the rear side of the motor as seen in Fig. 10. This can be explained by the air flow profile (Fig. 11). Due to the absence of an enclosure on the outside of the housing, the air mixes with the atmospheric air, thereby reducing the volume of air flowing past the rear side of the housing.

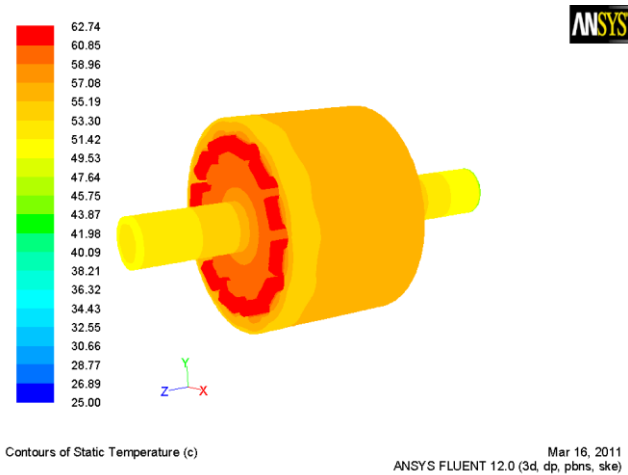


**Fig. 10.** Contours of temperature on the shaft, rotor, stator and windings.

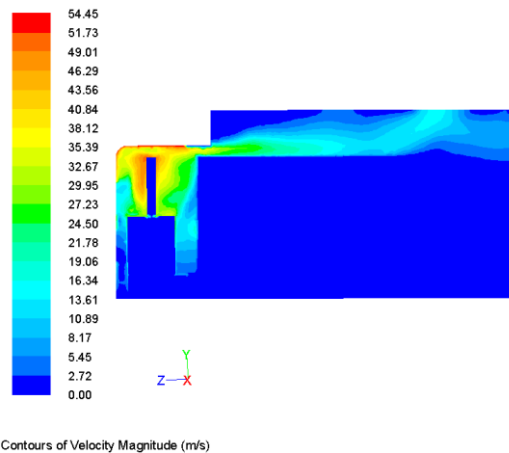


**Fig. 11.** Contours of air velocity on an axial cross-sectional plane of the motor.

From Fig. 11, it is evident that the flow is turbulent within the fan region and the

velocity reduces towards the rear side of the motor. The airflow profile also affects the wall heat transfer coefficient as shown in Fig. 12. This influences the rate of heat transfer between the housing and the flowing air and consequently influences the temperature distribution on the housing and the stator.

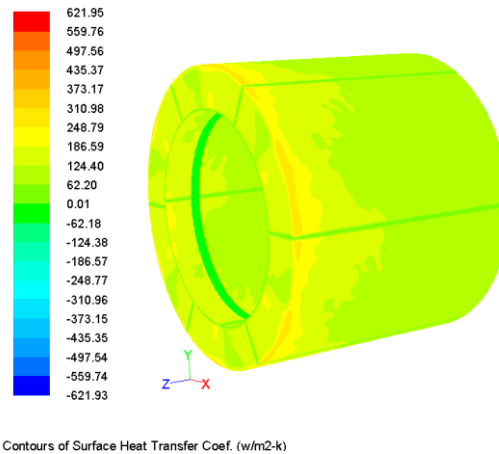


**Fig. 12.** Contours of surface heat transfer on the motor housing.

To study the effect of fin geometry on effective cooling of the motor, three other geometries of the housing (Fig. 13) were used. Other parameters of the motor were kept constant.

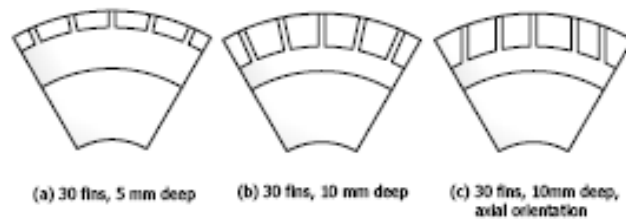
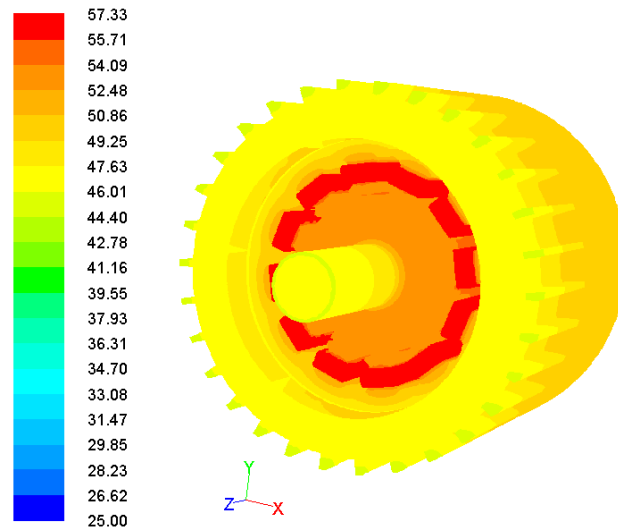


**Fig. 13.** Heat sink geometries.

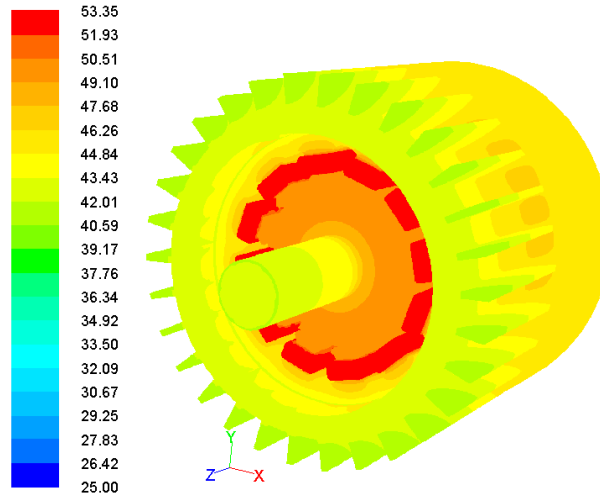
By introducing rectangular fins 2 mm thick and 5 mm deep, the highest temperature on the end windings is reduced by about 9%, as seen in Fig. 14. This is due to the increased surface area for convective heat transfer and reduced thickness of the housing wall which enhances conduction.



Contours of Static Temperature (c)

**Fig. 14.** Contours of temperature on critical motor components with introduction of fins.

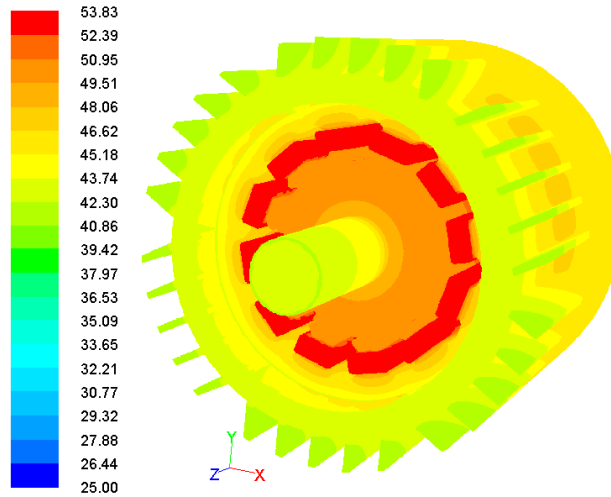
A further increase in the depth of the fins reduces the temperature of the windings by up to 15%. This is evident from Fig. 15. However, care should be taken in designing the fins so as not to compromise on the structural rigidity of the housing. As such, thermal-fluid-structural coupling in the motor should be studied.



Contours of Static Temperature (c)

**Fig. 15.** Contours of temperature on critical motor components with 10 mm deep fins on the motor housing.

The orientation of the fins did not have significant effect on the end winding temperature as seen in Fig. 16. In this case, fins of 10 mm depth, with axial orientation were used as opposed to the radial orientation considered previously.



Contours of Static Temperature (c)

**Fig. 16.** Contours of temperature on critical motor components with 10 mm depth

axial fins.

## **5 Conclusions and Future Work**

### **5.1 Conclusions**

CFD analysis has been conducted on a BLDC motor to study the thermal problem of the motor. The study incorporates the heat generated from electromagnetic losses and that generated from bearing frictional losses. The effect of housing geometry on heat dissipation is then evaluated. The results show that the highest temperature occurs at the end windings due to low heat transfer rate through the winding insulation and air gap both of which have low thermal conductivities. Though the highest temperature recorded is safe for the various classes of insulators, the study shows that CFD analysis can be used to optimize the thermal performance of high capacity electric vehicle motors such as those used for traction.

The effect of housing geometry was evaluated using three geometry designs and the results show that introduction of fins on the housing enhances heat transfer rate and the end winding temperature can be reduced by up to 15%.

The orientation of the fin has no significant effect on the maximum end winding temperature but may be considered as a design parameter for motor handling purposes or manufacturability.

The computational results also show that additional cooling within the winding region may be necessary in order to protect the insulation and to reduce the winding temperature which has a direct impact on the copper losses.

The CFD results provide an insight on the air-velocity profile on the housing, which is related to heat transfer coefficient. CFD can therefore be employed in the design of electric machines to improve thermal management of motors and also to reduce the design time.

### **5.2 Future Work**

There are a few aspects that can be incorporated to improve the analysis. Firstly, the thermal contact resistance due to the laminate structure of the stator and rotor should be evaluated in order to have a clear picture of the axial heat transfer.

Secondly, the use of different geometries such as parabolic, triangular, trapezoidal should be explored.

Thirdly, the effect of fan geometry should also be included in the design of motors to improve the flow and to reduce the power required to run the cooling fans.

Fourthly, the use of evaporative cooling should also be explored in the design of efficient cooling systems.

Finally, the CFD analysis should be verified using experimental work.

**Acknowledgments.** This work was supported by the program for the Training of Graduate Students in Green Car which is conducted by the Ministry of Commerce Industry and Energy of the Korean Government, Yeungnam University Research Support Program and Jomo Kenyatta University of Agriculture and Technology by awarding the author study leave.

## References

- [1] S. M. Jang, H. W. Cho, and S. K. Choi, "Design and Analysis of a High-Speed Brushless DC Motor for Centrifugal Compressor," *IEEE TRANSACTIONS ON MAGNETICS*, vol. 43, pp. 2573-2575, 2007.
- [2] C. Liao, C.-L. Chen, and T. Katcher, "Thermal Management of AC Induction Motors Using Computational Fluid Dynamics Modeling," *Institute of Electrical and Electronics Engineers, IEEE*, pp. 189-191, 1999.
- [3] P. Hwang and J. Kuria, "Estimation of Bearing Frictional Losses of Electric Vehicle Motor System," presented at the Korean Society of Tribologists and Lubrication Engineers (KSTLE), Seoul, S. Korea, 2010.
- [4] W. F. Arcier and L. Serillon, "Thermal Modelling of Permanent Magnet Motor for Traction," Master, KTH Royal Institute of Technology, 2007.
- [5] M. M. Baggu, H. L. Hess, and K. Rink, "Thermal Modeling of "Direct Lamination Cooling (DLC)" Induction Motor for Hybrid Electric Vehicle Applications," *Institute of Electrical and Electronics Engineers, IEEE*, pp. 242-246, 2005.
- [6] Y. Guo, J. G. Zhu, and W. Wu, "Thermal Analysis of Soft Magnetic Composite Motors Using a Hybrid Model With Distributed Heat Sources," *IEEE TRANSACTIONS ON MAGNETICS*, vol. 41, pp. 2124-2128, June 2005.
- [7] A. Boglietti, A. Cavagnino, and D. A. Staton, "Thermal Analysis of TEFC Induction Motors," presented at the Industry Applications Conference, 2004.
- [8] C. A. Cezario, *et al.*, "TRANSIENT THERMAL ANALYSIS OF AN INDUCTION ELECTRIC MOTOR," presented at the 18th International Congress of Mechanical Engineering, 2005.
- [9] Y. K. Chin and D. A. Staton, "TRANSIENT THERMAL ANALYSIS USING BOTH LUMPED CIRCUIT APPROACH AND FINITE ELEMENT METHOD OF A PERMANENT MAGNET TRACTION MOTOR," *SOUTH AFRICAN INSTITUTE OF ELECTRICAL ENGINEERS*, vol. 97, pp. 263-274, 2006.
- [10] G. Kylander, "Thermal modelling of small cage induction motors," PhD, Chalmers University of Technology, Göteborg, Sweden, 1995.
- [11] C. C. Chang, *et al.*, "Air cooling for a large-scale motor," *Applied Thermal Engineering*, vol. 30, pp. 1360-1368, 2010.
- [12] H. Li, "Flow driven by a stamped metal cooling fan – Numerical model and validation," *Experimental Thermal and Fluid Science*, vol. 33, pp. 683-694, 2009.

- [13] H. Li, "Cooling of a permanent magnet electric motor with a centrifugal impeller," *Journal of Heat and Mass Transfer*, vol. 53, pp. 797-810, 2010.
- [14] P. Andrada, *et al.*, "Power Losses in Outside-Spin Brushless D.C. Motors," Universitat Politecnica de Catalunya, Tech. Rep.2004.
- [15] B. J. Hamrock and W. J. Anderson, "Rolling - Element Bearing," National Aeronautics and Space Administration (NASA)1983.
- [16] F. E. Branch, "Keeping Motor Windings Dry," Facilities Engineering Branch, Denver Office, Denver, Colorado1991.
- [17] Y. A. Cengel, *Heat and Mass Transfer: A Practical Approach*, Third ed.: The McGraw-Hill Companies, 2007.